
¹⁸F-DCFPyL PET/CT in the Detection of Prostate Cancer at 60 and 120 Minutes: Detection Rate, Image Quality, Activity Kinetics, and Biodistribution

Maurits Wondergem^{1,2}, Friso M. van der Zant¹, Remco J.J. Knol¹, Sergiy V. Lazarenko¹, Jan Pruijm^{3,4}, and Igle J. de Jong²

¹Department of Nuclear Medicine, Noordwest Ziekenhuisgroep locatie Alkmaar, Alkmaar, The Netherlands; ²Department of Urology, University Medical Center Groningen, University of Groningen, Groningen, The Netherlands; ³Department of Nuclear Medicine and Molecular Imaging, University Medical Center Groningen, University of Groningen, Groningen, The Netherlands; and ⁴Department of Nuclear Medicine, Tygerberg Hospital, Stellenbosch University, Stellenbosch, South Africa

There is increasing interest in PET/CT with prostate-specific membrane antigen (PSMA) tracers for imaging of prostate cancer because of the higher detection rates of prostate cancer lesions than with PET/CT with choline. For ⁶⁸Ga-PSMA-11 tracers, late imaging at 180 min after injection instead of imaging at 45–60 min after injection improves the detection of prostate cancer lesions. For ¹⁸F-DCFPyL, improved detection rates have recently been reported in a small pilot study. In this study, we report the effects of PET/CT imaging at 120 min after injection of ¹⁸F-DCFPyL in comparison to images acquired at 60 min after injection in a larger clinical cohort of 66 consecutive patients with histopathologically proven prostate cancer. **Methods:** Images were acquired 60 and 120 min after injection of ¹⁸F-DCFPyL. We report the positive lesions specified for anatomic locations (prostate, seminal vesicles, local lymph nodes, distant lymph nodes, bone, and others) at both time points by visual analysis, the image quality at both time points, and a semiquantitative analysis of the tracer activity in both prostate cancer lesions as well as normal tissues at both time points. **Results:** Our data showed a significantly increasing uptake of ¹⁸F-DCFPyL between 60 and 120 min after injection in 203 lesions characteristic for prostate cancer (median, 10.78 vs. 12.86, $P < 0.001$, Wilcoxon signed-rank test). By visual analysis, 38.5% of all patients showed more lesions using images at 120 min after injection than using images at 60 min after injection, and in 9.2% a change in TNM staging was found. All lesions seen on images 60 min after injection were also visible on images 120 min after injection. A significantly better mean signal-to-noise ratio of 11.93 was found for images acquired 120 min after injection ($P < 0.001$, paired t test; signal-to-noise ratio at 60 min after injection, 11.15). **Conclusion:** ¹⁸F-DCFPyL PET/CT images at 120 min after injection yield a higher detection rate of prostate cancer characteristic lesions than images at 60 min after injection. Further studies are needed to elucidate the best imaging time point for ¹⁸F-DCFPyL.

Key Words: ¹⁸F-DCFPyL; PET/CT; prostate cancer; urology; image acquisition

J Nucl Med 2017; 58:1797–1804

DOI: 10.2967/jnumed.117.192658

In the Western world, prostate cancer has the highest incidence as compared with other cancers and the third highest mortality rate (European Cancer Observatory, <http://eu-cancer.iarc.fr/>). Imaging is an important pillar on which clinical decision making is based. For more than a decade, PET/CT has been one of the cornerstones of oncologic imaging and has been proven useful for a large number of malignancies. However, the most frequently used tracer ¹⁸F-FDG has a relatively low sensitivity for prostate cancer (1) and therefore PET/CT has had little impact on prostate cancer imaging and management until recently. This changed after the introduction of ¹⁸F-fluorocholine and ¹¹C-choline PET/CT, which is useful for detection and localization of prostate cancer and in clinical practice it is used especially for detection of a biochemical relapse after therapies with curative intent. The relatively low positive predictive values of ¹⁸F-fluorocholine and ¹¹C-choline, particularly due to false-positive inflammatory lymph nodes, has prevented the wide clinical use of those tracers in primary staging of prostate cancer. Another known drawback of choline tracers is the moderate sensitivity of those tracers for lymph node metastases (2).

Lack of specificity of conventional imaging techniques has encouraged screening of prostate cancer cells for possible antigens to develop agents capable of specific binding. This resulted in the development of monoclonal antibodies (mAbs) to target prostate-specific antigen (PSA) and prostatic acid phosphatase (3). Secretion of those antigens preclude cell-associated binding, and the presence of PSA and prostatic acid phosphatase in the plasma effectively blocks specific antibody binding at the tumor site. Later, prostate-specific membrane antigen (PSMA) was discovered (4,5); PSMA is a 750 amino acid transmembrane protein and a highly specific prostate epithelial cell membrane antigen (6). Physiologic expression of PSMA is 100–1,000 fold less than baseline expression in prostate cancer (7), and expression increases as tumor grade increases, with concurrent increase in metastatic sites and castration-refractory prostate cancer (8). Furthermore, PSMA is internalized and endosomally recycled, increasing the deposition of radiopharmaceuticals into the cell over time (9).

In 2006, ¹¹¹In-capromab, a mAb for targeting PSMA, was reported. However, this tracer has a poor efficacy associated with binding to the intracellular domain of PSMA, resulting in binding to nonviable cells, that have damaged cell membranes, only (10). A few years later, mAb targeting to the external domain of PSMA was reported. Because of the relatively large mass of mAbs, these

Received Mar. 1, 2017; revision accepted Apr. 11, 2017.
For correspondence or reprints contact: Maurits Wondergem, Noordwest Ziekenhuisgroep, Wilhelminalaan 12, 1815 JD, 0030, Alkmaar, The Netherlands.
E-mail: M.Wondergem@nwwz.nl
Published online Apr. 27, 2017.
COPYRIGHT © 2017 by the Society of Nuclear Medicine and Molecular Imaging.

ligands show slow clearance from background and slow target recognition, prohibiting their success as radiopharmaceuticals for imaging, because these are preferably administered and subsequently used for imaging on the same day. Furthermore, they require superior safety profiles, because mAbs have potential side effects including allergic reactions (11–13). From the late 2000s, small-molecule PSMA inhibitors, which are approximately 350-fold smaller than mAbs, have been reported (14–18). Those tracers have rapid target recognition and background clearance, and no adverse effects have been reported.

In comparison with choline PET/CT, these PSMA tracers have been shown to detect more lesions at lower PSA levels, increasing the sensitivity for prostate cancer and increasing the clinical impact of PET/CT in prostate cancer (17,19). Furthermore, the specific binding to PSMA increases specificity for prostate cancer and positive predictive values. Therefore, it is expected that these tracers may also be useful in primary staging, although scientific evidence for this is lacking at this point.

At the moment, PSMA tracers labeled with ^{68}Ga are primarily used in clinical practice; however, there is an increasing interest in ^{18}F -labeled PSMA tracers because of favorable physical and imaging characteristics. Positrons emitted by ^{18}F decay have lower kinetic energies as compared with those emitted by ^{68}Ga , resulting in a higher resolution of PET images acquired using ^{18}F tracers. Furthermore, the 110-min half-life of ^{18}F compared with 68 min for ^{68}Ga enables imaging at later time points without significant deterioration of image quality or the need for administration of higher dosages. Literature on PSMA tracer kinetics shows that the tracer accumulates in prostate cancer cells over time whereas background activity decreases (20–24). For ^{68}Ga -PSMA tracers, it has been reported that late imaging at 180 min after injection instead of imaging at 45–60 min after injection improves detection of prostate cancer lesions (25). In a recent pilot study published by Rowe et al., in 9 patients ^{18}F -DCFPyL, one of the available ligands for PSMA, demonstrated higher tumor radiotracer uptake and higher tumor-to-background ratios on images acquired 120 min after injection than images acquired 60 min after injection (26).

To build on these findings of improved lesion detection at later time points, we assessed whether image acquisition with ^{18}F -DCFPyL at 120 min after injection increases detection of lesions characteristic for prostate cancer. We studied the effects of PET/CT imaging at 120 min after injection of ^{18}F -DCFPyL in comparison to images acquired 60 min after injection in a clinical cohort of 66 consecutive patients with histopathologically proven prostate cancer.

MATERIALS AND METHODS

Patients

From November 3, 2016, 66 consecutive prostate cancer patients who were referred to our nuclear medicine department for ^{18}F -DCFPyL PET/CT were included in the study. ^{18}F -DCFPyL PET/CT was performed either for primary staging, localization of biochemical relapse after therapy with curative intent, or response measurement of systemic therapy. Follow-up scans of already included patients and those with deviations from the imaging protocol and scans of patients with known other malignancies except basal cell carcinoma of the skin were excluded. All patients gave written consent for the use of their anonymous data for scientific purposes. Besides the standard imaging protocol and clinical management, no additional measurements or actions affecting the patient were performed. The institutional review board approved this retrospective study, and the requirement to obtain informed consent was waived.

Imaging

^{18}F -DCFPyL was produced and synthesized by an on-site cyclotron and radiochemistry facility. Synthesis involves a 2-step reaction, in which first nucleophilic substitution by ^{18}F takes places on the leaving group of the precursor and second the protecting butyl groups are removed by acid hydrolysis. Purification of the compound was performed on a preparative high-performance liquid chromatography column as described by Boevet et al. (27).

Sixty and 120 min (± 5 min) after injection of 314 MBq of ^{18}F -DCFPyL (mean; range, 243–369 MBq; depending on body mass index [BMI]), PET images were acquired on a Siemens Biograph-16 TruePoint PET/CT scanner (Siemens Healthcare). At 60 min after injection, images were acquired from the inguinal region to the base of the skull (3 min per bed position). For logistic reasons, images were acquired from the inguinal region to the basal lung fields only at 120 min after injection. To compensate for radioactive decay, these images were acquired using a counting time of 5 min per bed position.

Reconstruction was done by means of an iterative 3-dimensional ordered-subsets expectation maximization algorithm using 4 iterations and 16 subsets and a 5-mm gaussian filter. Reconstructed images had an image matrix size of 256×256 , a pixel spacing of 2.67×2.67 mm, and a slice thickness of 4 mm.

For attenuation correction of the images 60 min after injection, a diagnostic CT with intravenous contrast administration was acquired using a tube current of 110 mAs at 110–130 kV (BMI < 25, 110 kV; BMI \geq 25, 130 kV), collimation of 16×1.2 mm, and a pitch of 0.95. A low-dose CT with intravenous contrast administration with a tube current of 25 mAs at 110 kV, collimation of 16×1.2 mm, and pitch of 0.95 was used for attenuation correction of images 120 min after injection. Both CT images were reconstructed using a slice thickness of 4 mm and a matrix size of 512×512 , resulting in voxel sizes of 1.37×1.37 mm for CT images used for attenuation correction and 0.98×0.98 mm for diagnostic CT images.

Lesion Selection and Data Extraction

For ^{18}F -DCFPyL PET/CT images acquired at both 60 and 120 min after injection, prostate cancer depositions with their accompanying anatomic location were scored by visual analysis by 2 experienced nuclear medicine physicians. The examined structures included prostate gland, seminal vesicles, local lymph nodes, distant lymph nodes, bone lesions, and other lesions. Local lymph nodes were defined as lymph nodes in the true pelvis, and lymph nodes from the aortic bifurcation and more cranially, as well as lymph nodes in the inguinal region, were defined as distant lymph nodes.

For lesions visible at both 60 and 120 min, activity (SUV_{max}) was measured by means of volume-of-interest (VOI) analysis (VOI iso-contour tool; 40% from maximum) using SyngoVia software (Siemens syngo.via; Siemens Healthcare) in a maximum of 4 lesions per anatomic location. For the prostate and seminal vesicles, only 1 measurement was done. Lesions directly adjacent to organs or tissues with normal tracer uptake with higher intensity than uptake in the target lesion were excluded from the analysis. When present, another lesion from the same anatomic location was included in the analysis.

Activity was also measured in normal tissues including blood, bone marrow, liver, spleen, duodenum, and kidneys using a standardized method (sphere VOI, except kidneys). Blood-pool activity was measured in the abdominal aorta, just cranially from the bifurcation; liver activity was measured in the right lobe in segment 5/6 (according to the Bismuth adaptation of the Couinaud classification of liver anatomy (28)); spleen activity was measured most laterally in the spleen; duodenal activity was measured in the segment directly anterior to the abdominal aorta; and bone marrow activity was measured in the vertebral body of L4.

Image quality was assessed by measuring the signal-to-noise ratio (SNR) in a sphere VOI of approximately 4 cm in the liver, which was

TABLE 1
Patient Characteristics

Characteristic	<i>n</i>
No. of patients	65
Indication ¹⁸ F-fluorocholine PET/CT	
Primary staging	21
Biochemical relapse	34
Therapy follow-up	8
Other	2
Mean age (y)	62 (range, 52–84)
Mean PSA at scanning (ng/mL)	56 (range, 0.1–1,481)
Gleason score	
6	4
7	16
8	18
9	10
Unknown	17
cT stage at diagnosis	
x	19
1	5
2	15
3a	18
3b	7
4	1
cN stage at diagnosis	
x	42
0	17
1	6
Previous therapy	
Prostatectomy	16
External radiation therapy	19
Brachytherapy	1
Previous salvage therapy	
External radiotherapy	7
High-intensity focused ultrasound	4
Patients on hormone therapy at scanning	
Yes	7
No	58

on visual inspection the most homogeneous organ, considering ¹⁸F-DCFPyL uptake, that was included in the field of view (FOV) at both time points. SNR was calculated by dividing the SUV_{mean} in the sphere VOI by the SD of the SUV in the sphere VOI.

Statistical Analysis

The Kolmogorov–Smirnov test was used to check for normal distribution of the data.

According to the presence or absence of normality, the paired *t* test or the Wilcoxon signed-rank test was used to test for statistically significant differences between SUV_{max} and SNR between the images acquired at 60 and 120 min after injection. Bland–Altman plots were used for graphical presentation of the data.

RESULTS

Patients

Between November 3, 2016, and January 26, 2017, 66 patients were included in the study. One patient was excluded because he received a deviant dose of ¹⁸F-DCFPyL. Therefore 65 patients were included in the analysis. Twenty-one patients were referred for ¹⁸FDCFPyL PET/CT for primary staging, 34 patients had a biochemical relapse after therapy with curative intent, 8 patients were scanned for therapy follow-up, and 2 patients were scanned for other reasons. Baseline patient characteristics are presented in Table 1.

Visual Analysis

In 6 patients, no enhanced ¹⁸F-DCFPyL uptake was detected. Five of those patients were scanned for biochemical relapse and had PSA values of 0.1, 0.2, 0.3, 0.5, and 0.6 ng/mL. The sixth patient was scanned on suspicion of biochemical relapse after radiation therapy; however, later PSA measurements showed a spontaneous PSA decrease (PSA from 4.4 to 3.0 ng/mL).

Enhanced ¹⁸F-DCFPyL uptake was encountered in 35 patients in the prostate, and in 13 patients uptake in a seminal vesicle or both vesicles was seen. All lesions were present at both time points. In general, the uptake was more demarcated on images acquired at 120 min after injection. Twelve of those patients (7 primary staging, 1 biochemical relapse, and 2 follow-up androgen-deprivation therapy) showed only increased uptake in the prostate, without signs of metastases.

Uptake in local and distant lymph nodes was seen in 31 and 14 patients at 60 min after injection and 34 and 17 patients at 120 min after injection, respectively. In 1 patient, referred for biochemical relapse after prostatectomy and salvage radiation therapy, both local and distant lymph nodes were seen on images at 120 min after injection only. In 2 patients, both staged for primary prostate cancer (T3aG19NxMx; initial PSA [iPSA], 35, and T3aG18NxMx; iPSA, 140, respectively), local lymph nodes were seen on late images only (Fig. 1). For 2 other patients, 1 referred for biochemical relapse after external radiation therapy (PSA, 7.0 ng/mL) and 1 for

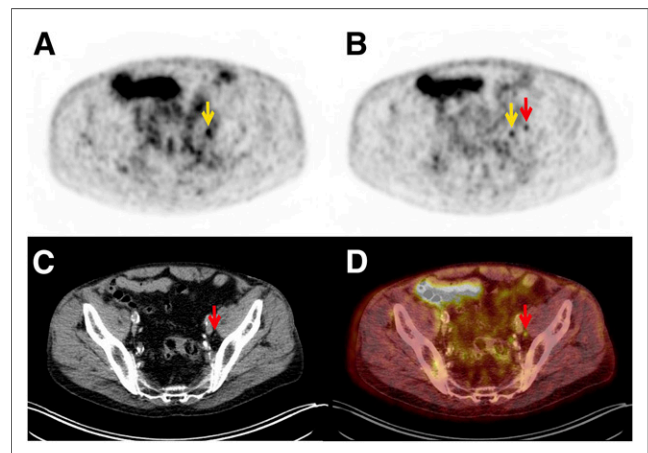


FIGURE 1. ¹⁸F-DCFPyL PET images at 60 min after injection (A) and 120 min after injection (B) of patient scanned for primary staging (T3aG19NxMx; iPSA, 35 ng/mL). Images show activity in ureter (yellow arrow). Additional focus with increased activity is seen on image acquired at 120 min after injection laterally from ureter and dorsally from left external iliac artery (red arrow). CT (C) and fused PET/CT (D) images show small lymph node, which corresponds with focally increased ¹⁸F-DCFPyL uptake at 120 min after injection (red arrow).

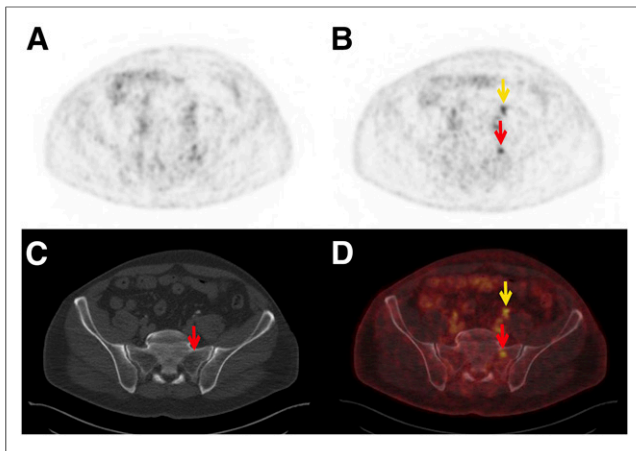


FIGURE 2. ^{18}F -DCFPyL PET images 60 min after injection (A) and 120 min after injection (B) of patient with biochemical relapse after prostatectomy (PSA, 5.2 ng/mL). Images show clearly increased ^{18}F -DCFPyL uptake at 120 min after injection (red arrow), which was not scored as lesion characteristic of prostate cancer at 60 min after injection. Activity in left ureter is also seen only on images 120 min after injection (yellow arrow). (C) CT images showed no anatomic substrate. (D) Fused PET/CT images showed anatomic location of increased uptake in sacral bone.

primary staging (T1G18NxMx; iPSA, 68), late images showed both local and distant lymph node metastases, whereas early images showed only local lymph nodes. Regarding lesions in the FOV of both scans, all lymph nodes seen on images at 60 min after injection were also seen on images at 120 min after injection, whereas images at 120 min after injection showed more positive local lymph nodes in 16 patients and more positive distant lymph nodes in 7 patients as compared with images at 60 min after injection.

Enhanced ^{18}F -DCFPyL uptake in skeletal lesions was seen in 21 patients at 60 min after injection and in 17 patients at 120 min after injection. For 5 patients, the skeletal lesions seen on images at 60 min after injection were outside the FOV of the images at 120 min after injection. For 1 patient, referred for biochemical relapse after prostatectomy (PSA, 5.2 ng/mL), images at 60 min after injection showed no lesions with enhanced uptake, whereas images at 120 min after injection showed enhanced uptake in a solitary lesion in the sacrum (Fig. 2). Regarding lesions in the FOV of both scans, all skeletal lesions detected at 60 min after injection were also visible on images acquired at 120 min after injection, whereas in 8 patients more bone lesions were seen at 120 min after injection. In 1 patient with already-known plural prostate cancer metastases, increased ^{18}F -DCFPyL was found in these lesions, whereas no increased activity in other organs was found. In a total of 25 patients (38.5%), the images at 120 min after injection showed more lesions with enhanced ^{18}F -DCFPyL uptake than the images at 60 min after injection, and all lesions visible on images at 60 min after injection were also visible at 120 min after injection.

According to the presently used TNM classification (7th ed.), 6 patients (9.2%) had a higher disease stage on images at 120 min after injection than on images at 60 min after injection. One patient was upstaged from N0M0 to N1M1a, 2 patients from N0M0 to N1M0, 2 patients from N1M0 to N1M1a, and 1 patient from N0M0 to N0M1b.

Quantitative Analysis

From 59 patients, a total of 203 lesions characteristic for prostate cancer with enhanced ^{18}F -DCFPyL uptake, visible at both

imaging time points, were included in the analysis. Thirty prostate lesions, 6 seminal vesicle lesions, 125 lymph nodes (81 local and 44 distant lymph nodes), and 42 skeletal lesions were included in the quantitative analysis. Five prostate lesions and 7 seminal vesicle lesions were excluded because these could not be clearly delineated from urine activity in the bladder or urethra, or in the case of seminal vesicle lesions, extension from the prostate into seminal vesicles was considered as 1 lesion for quantitative analysis.

Overall, a statistically significant increase in uptake over time was seen in the 203 lesions with enhanced ^{18}F -DCFPyL uptake characteristic for prostate cancer (Fig. 3). Median SUV_{max} increased from 10.8 to 12.9 ($P < 0.001$, Wilcoxon signed-rank test). Also for all individual anatomic regions, including prostate, seminal vesicles, local lymph nodes, distant lymph nodes, and skeletal lesions, an overall significant increase in ^{18}F -DCFPyL uptake over time was found (Table 2). In 6 of 203 lesions, decreasing PSMA uptake was observed. One prostate lesion, 1 bone lesion, and 4 lymph nodes showed a decrease in SUV_{max} of -0.16 , -0.16 , -0.05 , -0.04 , -0.16 , and -0.26 , respectively.

Quantitative analysis of normal uptake of ^{18}F -DCFPyL in the liver, spleen, duodenum, blood pool, and bone marrow was measured in 65, 63, 65, 62, and 62 patients, respectively (Fig. 4). In 2 patients, activity in the spleen could not be measured because of previous splenectomy. In 3 patients, blood-pool activity could not be measured accurately because of high activity in lymph nodes in the direct vicinity of the aorta. Bone marrow activity could not be measured in 3 patients who had metastases in the vertebral body of L4.

In all patients, ^{18}F -DCFPyL activity in the blood pool, bone marrow, and spleen decreased significantly over time ($P < 0.001$, Table 2). Uptake in the liver and duodenum showed a variable course over time on a per-patient basis (Fig. 4); however, by

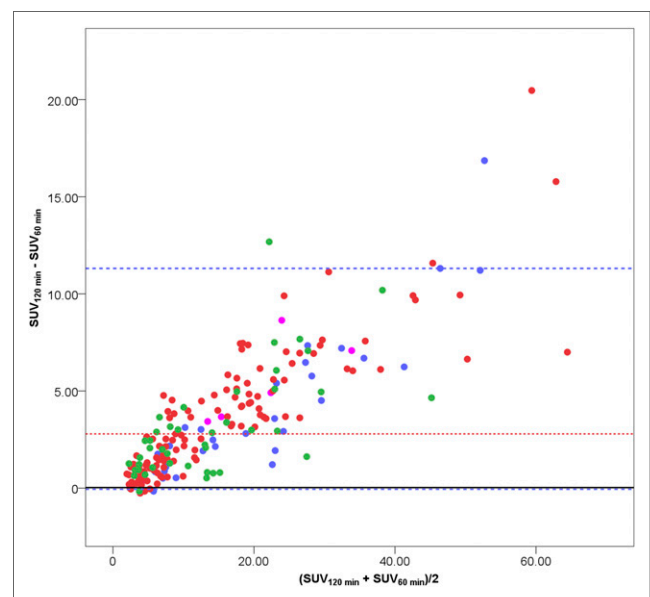


FIGURE 3. Bland-Altman plot. Difference between ^{18}F -DCFPyL activity at 120 and 60 min after injection in lesions characteristic of prostate cancer is plotted against mean activity in each lesion. Plotted as red dotted line is median activity difference in entire cohort, and blue dotted lines are 95% limits of agreement. Blue dots = prostate lesions; purple dots = seminal vesicle lesions; red dots = lymph nodes; green dots = skeletal lesions.

TABLE 2
Comparison of ¹⁸F-DCFPyL Uptake (SUV_{max}) 60 and 120 Minutes After Injection in Different Tissues

Tissue	<i>n</i>	Acquisition time (min after injection)	Mean or median SUV _{max}	SD or interquartile range	<i>P</i>
Malignant					
All lesions	203	60	10.78*	14.57 [†]	<0.001 [‡]
		120	12.86*	18.08 [†]	
Prostate	30	60	19.17	12.28	<0.001 [¶]
		120	23.27	15.77	
Vesicles	6	60	16.57*	12.67 [†]	0.028 [‡]
		120	21.03*	18.01 [†]	
Lymph nodes total	125	60	8.65*	13.34 [†]	<0.001 [‡]
		120	11.05*	17.13 [†]	
Local lymph nodes	81	60	7.48*	14.31 [†]	<0.001 [‡]
		120	10.25*	17.93 [†]	
Distant lymph nodes	44	60	10.77*	11.58 [†]	<0.001 [‡]
		120	14.27*	15.18 [†]	
Osseous	42	60	11.00*	14.19 [†]	<0.001 [‡]
		120	12.83*	18.72 [†]	
Normal					
Liver	65	60	6.96*	1.68 [†]	0.520 [‡]
		120	6.93*	1.41 [†]	
Spleen	63	60	5.96	2.16	<0.001 [¶]
		120	4.78	1.73	
Kidney	64	60	48.05*	19.65 [†]	<0.001 [‡]
		120	41.63*	20.29 [†]	
Duodenum	65	60	10.79*	5.06 [†]	<0.001 [‡]
		120	12.41*	6.42 [†]	
Blood pool	62	60	1.85*	0.47 [†]	<0.001 [‡]
		120	1.41*	0.46 [†]	
Bone marrow	62	60	1.26	0.29	<0.001 [¶]
		120	0.99	0.18	

For data not normally distributed: *median and [†]interquartile range. [‡]Wilcoxon signed-rank test. For data normally distributed: mean, SD, and [¶]Paired *t* test.

statistical analysis a significant increase in the mean SUV_{max} over time was found in the duodenum and a significant decrease in the right kidney.

Image Quality

The SNR, as measured in the liver in all 65 included patients, showed a variable course over time on a per-patient basis (Fig. 5). However, by statistical analysis a significantly better mean SNR at 120 min after injection of 11.93 was found (*P* < 0.001, paired *t* test; SNR at 60 min after injection, 11.15).

DISCUSSION

Our data demonstrated a higher detection rate of lesions characteristic of prostate cancer on images acquired at 120 min after injection than 60 min after injection. According to the presently used TNM classification (7th ed.), 6 patients (9.2%) had a higher disease stage on images at 120 min after injection than on images at

60 min after injection. Some changes in clinical management were not reflected by the TNM stage and therefore the true clinical impact may be even higher than a change in management in 9.2% of patients. For example, detection of more local lymph nodes may change the radiation field for T2c-4N1M0 tumors suitable for radiation therapy with curative intent (Fig. 6), and the detection of more suspected local or distant lymph nodes in the case of biochemical failure may change the extent of a salvage lymph node dissection or may result in abstention from surgery and start of palliative systemic therapy instead. The exact impact on clinical management was beyond the scope of this study.

For ⁶⁸Ga-PSMA-11 PET/CT, increased lesion detection has been shown in a recent retrospective study by Afshar-Oromieh et al. (25). They found a better detection rate of lesions characteristic for prostate cancer at 180 min after injection of ⁶⁸Ga-PSMA-11 than at 60 min after injection in a cohort of 112 patients with prostate cancer. In 4 patients (3.6%), they found lesions on late imaging

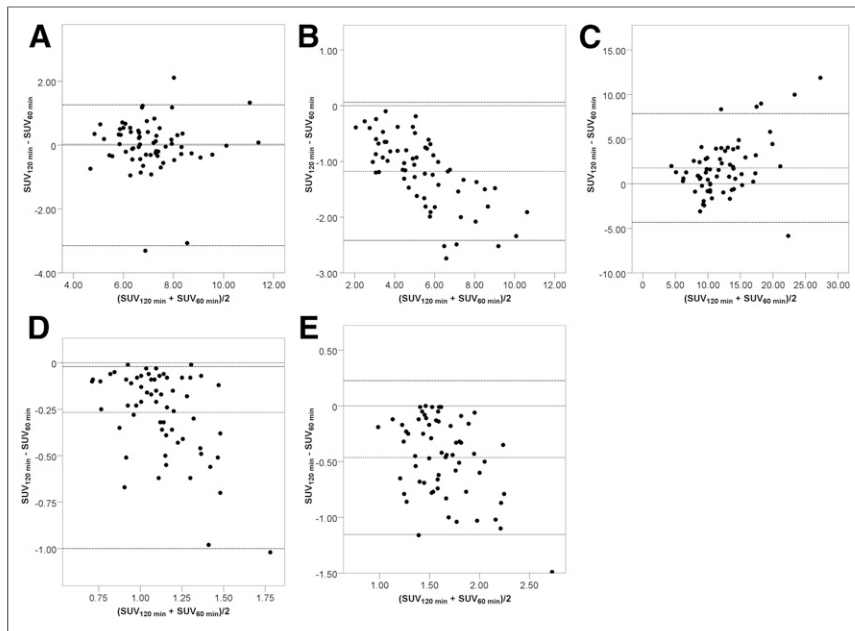


FIGURE 4. Bland–Altman plots. Differences between normal ^{18}F -DCFPyL activity at 120 and 60 min after injection in different tissues plotted against mean activity in each tissue ([A] liver, [B] spleen, [C] duodenum, [D] blood pool, [E] bone marrow). Plotted dotted line is mean or median activity difference in entire cohort, and striped lines are 95% limits of agreement. Mean activity is given for data normally distributed (spleen, duodenum, blood pool) and median activity for data with nonnormal distribution (liver, bone marrow).

whereas early images showed no lesions characteristic of prostate cancer. In 8 patients, they found 1 unclear lesion on images 60 min after injection, which was clarified on the images at 180 min after injection. Furthermore, they found a higher SUV_{max} and contrast

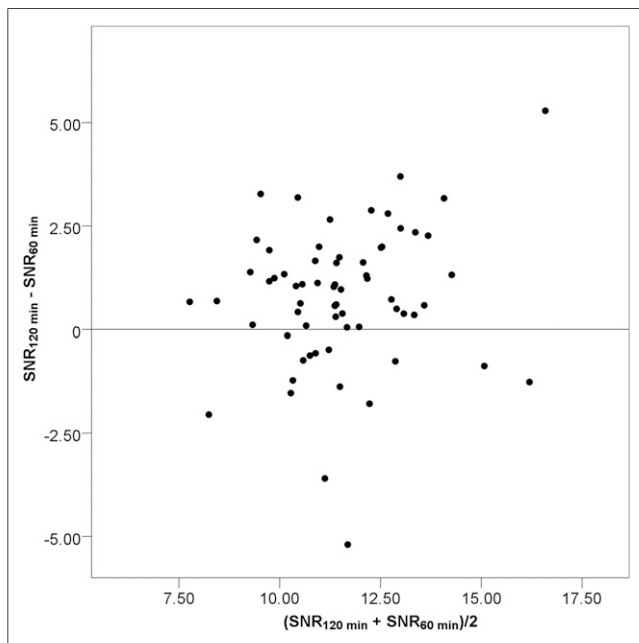


FIGURE 5. Bland–Altman plot. Difference between SNRs measured in liver at 60 and 120 min after injection plotted against mean SNR in each patient. Plotted dotted line is mean SNR difference in entire cohort, and striped lines are 95% limits of agreement.

on late images in most patients. These findings are largely in line with our findings.

However, Afshar-Oromieh et al. (25) also found 12 patients with possible prostate cancer lesions, which could not be confirmed on late scans, and 2 patients showed a lesion characteristic of prostate cancer on early images, which was not detectable at 180 min after injection because of low contrast. In our cohort, we found 6 lesions with a slight decrease in SUV_{max} over time; however, we found no lesions visible 60 min after injection that were no longer detectable on later scans. Several factors may explain this difference. First, there is a difference between the time point of image acquisition of the late scan, being 120 min after injection in our cohort compared with 180 min after injection in the cohort presented by Afshar-Oromieh et al. (25). Second, different tracers were used, which may have slightly different biodistribution and biokinetics. Third, there may be differences in the included patient populations, because Afshar-Oromieh et al. included mainly patients who showed unclear findings, which may be a more challenging cohort that includes more patients with lesions presenting with low or decreasing PSMA tracer uptake.

Conversely, our cohort included all patients referred for ^{18}F -DCFPyL PET/CT. A fourth difference is the used radioactive isotope ^{68}Ga in the PSMA tracer in the study by Afshar-Oromieh et al. as compared with ^{18}F in the present study. In general, the half-life of 110 min for ^{18}F is more suitable for imaging at later time points than the 68-min half-life of ^{68}Ga ; however, the visualization of prostate cancer lesions was shown to be independent from the short half-life of ^{68}Ga within a time window of 4 h after injections of approximately 150 MBq of ^{68}Ga -PSMA-11 in another paper by Afshar-Oromieh et al. (24).

As mentioned before, we found lesions with decreasing ^{18}F -DCFPyL uptake over time. Also, other studies showed decreasing PSMA tracer uptake over time in a minority of lesions (21,25,29). Afshar-Oromieh et al. speculated that decreasing uptake may be caused by a reduced internalization rate of PSMA ligands. In our cohort, we found only slight decreasing activity in 6 small lesions. Therefore, the observed decreasing activity in our cohort may also have contributed to technique-related partial-volume effects. All lesions with decreasing uptake over time were still clearly visible at 120 min after injection.

Our data show that ^{18}F -DCFPyL uptake in normal tissue such as the spleen, bone marrow, and blood pool decreases significantly over time in all patients. Activity in the liver shows no significant change over time. Given the increase in ^{18}F -DCFPyL uptake in suspected malignant lesions, this results in better tumor-to-background ratios. This underpins our finding of better lesion detection on images acquired at 120 min after injection. The uptake in the duodenum shows a significant increase in mean SUV_{max} , which may be an argument for image acquisition at an earlier time point. However, for several reasons an earlier acquisition time would probably not affect lesion detection. First, there is a large interpatient variability in duodenal uptake over time, and 27.7% of the patients

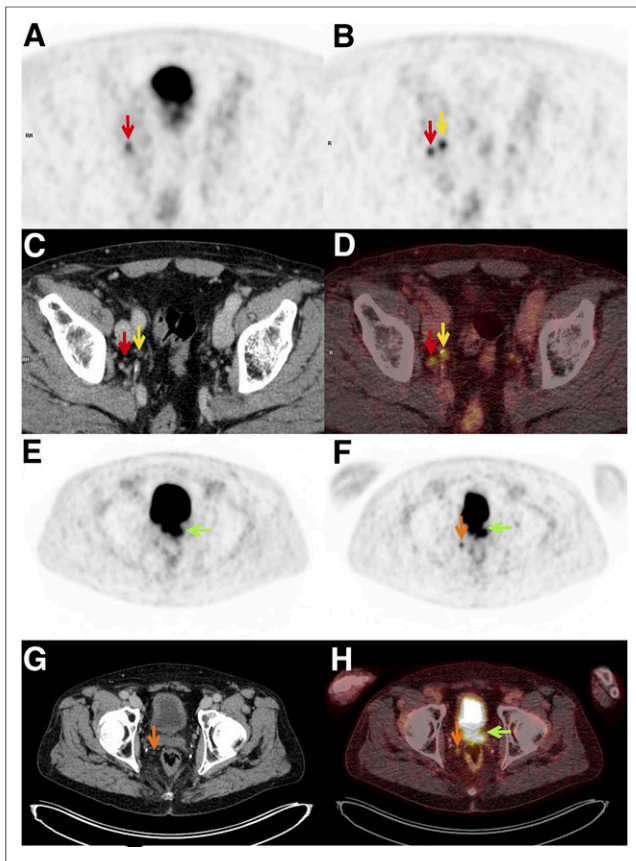


FIGURE 6. ^{18}F -DCFPyL PET/CT of patient scanned for primary staging (T2G19NxMx; iPSA, 34 ng/mL). PET images at 60 min after injection (A) and 120 min after injection (B) show focally increased uptake in right obturator fossa (red arrow), which corresponds to small lymph node on CT (C) and fused PET/CT (D) images. PET images at 120 min after injection (F) additionally show focal uptake laterally from rectum (orange arrow), which was not seen at 60 min after injection (E), corresponding to small lymph node on CT (G) and fused PET/CT (F) images. Activity in right ureter was seen on images at 120 min after injection only (yellow arrow), and at both time points activity in prostate was detected (green arrow, E, F, and H). Additionally (not shown) focally increased uptake in right costa 8 was found at both time points. Before ^{18}F -DCFPyL PET/CT, brachytherapy was scheduled for this patient, but after PET/CT patient was referred for radiation therapy on prostate, local lymph nodes, and solitary bone metastasis.

in the present cohort showed decreasing activity over time. Second, the mean SUV_{max} of the duodenum exceeded the mean SUV_{max} in distant lymph nodes at both time points, and therefore duodenal activity interfered with detection of small lymph node metastases in the vicinity of the duodenum at both time points. Third, prostate cancer lesions adjacent to the duodenum are rare and even more rarely exist without the presence of other lesions at other locations. Therefore, a change of the therapeutic procedure by lesions adjacent to the duodenum was unlikely.

Initially, we intended to measure ^{18}F -DCFPyL activity in the kidney over time as well. However, high activity in the urinary bladder and ureters was seen in many patients at both 60 and 120 min after injection. Therefore, we initiated administration of diuretics to reduce activity in the urinary tract and effectuate better interpretability of the prostate region and lymph nodes adjacent to ureters. Because an effect of diuretics on SUVs in the kidneys was found, we excluded the SUV measurements in the kidneys from the analysis.

For practical reasons, the FOV of the images at 120 min after injection was smaller than the FOV of the images acquired at 60 min after injection to enable acquisition of both scans in time frames of 30 min. Five bone lesions visible on images at 60 min after injection were not in the FOV of the images 120 min after injection. Strictly it cannot be ruled out that those lesions became undetectable on the images at 120 min after injection; however, this is highly unlikely given the findings in lesions visible at both time points. On the other hand, it is also possible that we missed additional lesions outside the FOV of the images at 120 min after injection.

Imaging at 120 min after injection may be a logistic challenge for nuclear medicine departments because most schedules are appointed on image acquisition 60 min after injection as is the current practice for ^{18}F -FDG PET/CT. A doubling of the waiting time doubles the number of shielded rooms needed for patient preparation. A longer waiting time could be a trade-off between the benefits according to the SNR and the signal quality due to radioactive decay of the tracer. Consequently, we extended the counting time per bed position 120 min after injection by 120 s (3 vs. 5 min, respectively) to compensate for decay, which comes with the cost of valuable camera time. Given the excellent SNRs at both time points, it could be possible to shorten the counting time at 120 min after injection. This is also supported by a previous study with ^{68}Ga -PSMA-11, in which imaging at later time points without adjustments of counting times showed superior image quality for images 180 min after injection in comparison to images 60 min after injection (21). Because of the pharmacokinetics of PSMA ligands, the decay of the radioisotope seems not essential for PET imaging with PSMA tracers in a time window of at least 3 h. Although there are practical challenges as mentioned above, the higher diagnostic outcome of images at 120 min after injection, as found in our data, should be a leading factor in decision making regarding scan protocols. Waiting times of more than 120 min after injection of ^{18}F -DCFPyL may even result in a better detection rate.

A potential limitation of our study is the use of CT with diagnostic properties and intravenous contrast for attenuation correction for the images 60 min after injection, whereas attenuation correction for images 120 min after injection was done with a low-dose CT without intravenous contrast. Literature on the effects of intravenous contrast-enhanced CT on SUV measurements in ^{18}F -DCFPyL PET/CT is absent. However, the used technique is similar to ^{18}F -FDG PET/CT. Studies on this topic in ^{18}F -FDG PET/CT have shown that the clinical impact of contrast-enhanced CT on SUV measurements is absent or negligible (30–32). The standardization protocol for ^{18}F -FDG PET/CT by Boellaard et al., however, advises that no contrast agent should be used until it has been established that attenuation artifacts are completely absent when used during attenuation-corrected CT (33). Because the ^{18}F -DCFPyL PET/CT images were acquired in a standard clinical setting and given the advantages of enhanced CTs with intravenous contrast, especially the characterization of lymph nodes adjacent to vascular structures or ureters, total-body images at 60 min after injection were acquired in combination with intravenous contrast-enhanced CT. SUVs measured in tissue that show contrast enhancement such as the lymph nodes, blood pool, spleen, and liver may therefore be somewhat higher in the early phase. In lesions characteristic for prostate cancer, we found a significant increase in SUV_{max} over time. If intravenous contrast affected the SUV measurements, the found difference would be even higher in reality.

Another limitation of the presented data is the lack of a reference with the accepted gold standard, which is histopathologic confirmation of the included lesions. However, it is practically impossible and ethically inappropriate to get histopathologic confirmation of all lesions included in this study. Furthermore, PSMA tracers with ^{68}Ga have been proven to be highly specific for prostate cancer, and therefore lesions with increased ^{18}F -DCFPyL, which fit the pattern of metastatic spread of prostate cancer, should be considered as highly suggestive of prostate cancer (34–36).

CONCLUSION

Our data show a significantly increasing uptake of ^{18}F -DCFPyL between 60 and 120 min after injection in lesions characteristic for prostate cancer. In 38.5% of all patients more lesions are seen, and in 9.2% a change in TNM staging is found using images 120 min after injection as compared with 60 min after injection.

Further studies are needed to elucidate the best imaging time point for ^{18}F -DCFPyL.

DISCLOSURE

No potential conflict of interest relevant to this article was reported.

ACKNOWLEDGMENT

We thank Tjeerd van der Ploeg, PhD, Foreest Medical School, Noordwest Ziekenhuisgroep, Alkmaar, for his help with the statistical analysis.

REFERENCES

- Jadvar H. Imaging evaluation of prostate cancer with ^{18}F -fluorodeoxyglucose PET/CT: utility and limitations. *Eur J Nucl Med Mol Imaging*. 2013;40(suppl 1):S5–S10.
- Evangelista L, Guttilla A, Zattoni F, Muzzio PC, Zattoni F. Utility of choline positron emission tomography/computed tomography for lymph node involvement identification in intermediate- to high-risk prostate cancer: a systematic literature review and meta-analysis. *Eur Urol*. 2013;63:1040–1048.
- Ghosh A, Heston WD. Tumor target prostate specific membrane antigen (PSMA) and its regulation in prostate cancer. *J Cell Biochem*. 2004;91:528–539.
- Pinto JT, Suffoletto BP, Berzin TM, et al. Prostate-specific membrane antigen: a novel folate hydrolase in human prostatic carcinoma cells. *Clin Cancer Res*. 1996;2:1445–1451.
- Israeli RS, Powell CT, Corr JG, Fair WR, Heston WD. Expression of the prostate-specific membrane antigen. *Cancer Res*. 1994;54:1807–1811.
- Rajasekaran AK, Anilkumar G, Christiansen JJ. Is prostate-specific membrane antigen a multifunctional protein? *Am J Physiol Cell Physiol*. 2005;288:C975–C981.
- Sokoloff RL, Norton KC, Gasior CL, Marker KM, Grauer LS. A dual-monoclonal sandwich assay for prostate-specific membrane antigen: levels in tissues, seminal fluid and urine. *Prostate*. 2000;43:150–157.
- Laidler P, Dulinska J, Lekka M, Lekki J. Expression of prostate specific membrane antigen in androgen-independent prostate cancer cell line PC-3. *Arch Biochem Biophys*. 2005;435:1–14.
- Rajasekaran SA, Anilkumar G, Oshima E, et al. A novel cytoplasmic tail MXXXL motif mediates the internalization of prostate-specific membrane antigen. *Mol Biol Cell*. 2003;14:4835–4845.
- Elsässer-Beile U, Wolf P, Gierschner D, Buhler P, Schultze-Seemann W, Wetterauer U. A new generation of monoclonal and recombinant antibodies against cell-adherent prostate specific membrane antigen for diagnostic and therapeutic targeting of prostate cancer. *Prostate*. 2006;66:1359–1370.
- Tagawa ST, Beltran H, Vallabhajosula S, et al. Anti-prostate-specific membrane antigen-based radioimmunotherapy for prostate cancer. *Cancer*. 2010;116:1075–1083.
- Wolf P, Freudenberg N, Buhler P, et al. Three conformational antibodies specific for different PSMA epitopes are promising diagnostic and therapeutic tools for prostate cancer. *Prostate*. 2010;70:562–569.

- Regino CA, Wong KJ, Milenic DE, et al. Preclinical evaluation of a monoclonal antibody (3C6) specific for prostate-specific membrane antigen. *Curr Radiopharm*. 2009;2:9–17.
- Foss CA, Mease RC, Fan H, et al. Radiolabeled small-molecule ligands for prostate-specific membrane antigen: in vivo imaging in experimental models of prostate cancer. *Clin Cancer Res*. 2005;11:4022–4028.
- Mease RC, Dusich CL, Foss CA, et al. *N*-[*N*-(*S*)-1,3-dicarboxypropyl]carbamoyl]-4-[^{18}F]fluorobenzyl-L-cysteine, [^{18}F]DCFPyL: a new imaging probe for prostate cancer. *Clin Cancer Res*. 2008;14:3036–3043.
- Chen Y, Pullambhatla M, Foss CA, et al. 2-(3-{1-carboxy-5-[(6-[^{18}F]fluoro-pyridine-3-carbonyl)-amino]-pentyl]-ureido)-pen taneedioic acid, [^{18}F]DCFPyL, a PSMA-based PET imaging agent for prostate cancer. *Clin Cancer Res*. 2011;17:7645–7653.
- Afshar-Oromieh A, Zechmann CM, Malcher A, et al. Comparison of PET imaging with a ^{68}Ga -labelled PSMA ligand and ^{18}F -choline-based PET/CT for the diagnosis of recurrent prostate cancer. *Eur J Nucl Med Mol Imaging*. 2014;41:11–20.
- Eder M, Neels O, Muller M, et al. Novel preclinical and radiopharmaceutical aspects of [^{68}Ga]ga-PSMA-HBED-CC: a new PET tracer for imaging of prostate cancer. *Pharmaceuticals (Basel)*. 2014;7:779–796.
- Bluemel C, Krebs M, Polat B, et al. ^{68}Ga -PSMA-PET/CT in patients with biochemical prostate cancer recurrence and negative ^{18}F -choline-PET/CT. *Clin Nucl Med*. 2016;41:515–521.
- Szabo Z, Mena E, Rowe SP, et al. Initial evaluation of [^{18}F]DCFPyL for prostate-specific membrane antigen (PSMA)-targeted PET imaging of prostate cancer. *Mol Imaging Biol*. 2015;17:565–574.
- Afshar-Oromieh A, Malcher A, Eder M, et al. PET imaging with a [^{68}Ga]gallium-labelled PSMA ligand for the diagnosis of prostate cancer: biodistribution in humans and first evaluation of tumour lesions. *Eur J Nucl Med Mol Imaging*. 2013;40:486–495.
- Herrmann K, Bluemel C, Weineisen M, et al. Biodistribution and radiation dosimetry for a probe targeting prostate-specific membrane antigen for imaging and therapy. *J Nucl Med*. 2015;56:855–861.
- Afshar-Oromieh A, Hetzheim H, Kratochwil C, et al. The theranostic PSMA ligand PSMA-617 in the diagnosis of prostate cancer by PET/CT: biodistribution in humans, radiation dosimetry, and first evaluation of tumor lesions. *J Nucl Med*. 2015;56:1697–1705.
- Afshar-Oromieh A, Hetzheim H, Kubler W, et al. Radiation dosimetry of ^{68}Ga -PSMA-11 (HBED-CC) and preliminary evaluation of optimal imaging timing. *Eur J Nucl Med Mol Imaging*. 2016;43:1611–1620.
- Afshar-Oromieh A, Sattler LP, Mier W, et al. The clinical impact of additional late PET/CT imaging with ^{68}Ga -PSMA-11 (HBED-CC) in the diagnosis of prostate cancer. *J Nucl Med*. 2017;58:750–755.
- Rowe SP, Macura KJ, Mena E, et al. PSMA-based [^{18}F]DCFPyL PET/CT is superior to conventional imaging for lesion detection in patients with metastatic prostate cancer. *Mol Imaging Biol*. 2016;18:411–419.
- Bouvet V, Wuest M, Jans HS, et al. Automated synthesis of [^{18}F]DCFPyL via direct radiofluorination and validation in preclinical prostate cancer models. *EJNMMI Res*. 2016;6:40-016-0195-6.
- Bismuth H. Surgical anatomy and anatomical surgery of the liver. *World J Surg*. 1982;6:3–9.
- Sahlmann CO, Meller B, Bouter C, et al. Biphasic ^{68}Ga -PSMA-HBED-CC-PET/CT in patients with recurrent and high-risk prostate carcinoma. *Eur J Nucl Med Mol Imaging*. 2016;43:898–905.
- Verburg FA, Kuhl CK, Pietsch H, Palmowski M, Mottaghy FM, Behrendt FF. The influence of different contrast medium concentrations and injection protocols on quantitative and clinical assessment of FDG-PET/CT in lung cancer. *Eur J Radiol*. 2013;82:e617–e622.
- Aschoff P, Plathow C, Beyer T, et al. Multiphase contrast-enhanced CT with highly concentrated contrast agent can be used for PET attenuation correction in integrated PET/CT imaging. *Eur J Nucl Med Mol Imaging*. 2012;39:316–325.
- Mawlawi O, Erasmus JJ, Munden RF, et al. Quantifying the effect of IV contrast media on integrated PET/CT: clinical evaluation. *AJR*. 2006;186:308–319.
- Boellaard R. Standards for PET image acquisition and quantitative data analysis. *J Nucl Med*. 2009;50(suppl 1):11S–20S.
- Herlemann A, Wenter V, Kretschmer A, et al. ^{68}Ga -PSMA positron emission tomography/computed tomography provides accurate staging of lymph node regions prior to lymph node dissection in patients with prostate cancer. *Eur Urol*. 2016;70:553–557.
- Rauscher I, Maurer T, Beer AJ, et al. Value of ^{68}Ga -PSMA HBED-CC PET for the assessment of lymph node metastases in prostate cancer patients with biochemical recurrence: comparison with histopathology after salvage lymphadenectomy. *J Nucl Med*. 2016;57:1713–1719.
- Afshar-Oromieh A, Avtzi E, Giesel FL, et al. The diagnostic value of PET/CT imaging with the ^{68}Ga -labelled PSMA ligand HBED-CC in the diagnosis of recurrent prostate cancer. *Eur J Nucl Med Mol Imaging*. 2015;42:197–209.